

## Article

# Recovery of Rare Earth Elements from Spent NdFeB-Magnets: Separation of Iron through Reductive Smelting of the Oxidized Material (Second Part)

Hanwen Chung <sup>1</sup>, Srecko Stopic <sup>1,\*</sup>, Elif Emil-Kaya <sup>1,2,3</sup>, Sebahattin Gürmen <sup>2</sup>  and Bernd Friedrich <sup>1</sup> <sup>1</sup> IME Process Metallurgy and Metal Recycling, RWTH Aachen University, 52056 Aachen, Germany<sup>2</sup> Department of Metallurgical & Materials Engineering, Istanbul Technical University, 34469 Istanbul, Turkey<sup>3</sup> Department of Materials Science and Technology, Turkish-German University, 34820 Istanbul, Turkey

\* Correspondence: sstopic@ime-aachen.de; Tel.: +49-17678261674

**Abstract:** This paper proposes a pyrometallurgical recycling method for end-of-life NdFeB magnets by oxidizing them in air and subsequently smelting them. The smelting process enabled the recovery of rare earth elements (REEs), producing a new reach concentrate separating the iron as a metallic phase. From the products of smelting, the metallic phase showed a maximum Fe content of 92.3 wt.%, while the slag phase showed a maximum total REE (Nd, Pr, and Dy) content of 47.47 wt.%, both at a smelting temperature of 1500 °C. ICE-OES and XRD analysis were conducted on both phases, and results showed that the metal phase consists mainly of Fe and Fe<sub>3</sub>C while the slag phase consists of the RE-oxides, leftover Fe<sub>2</sub>O<sub>3</sub>, and a mixture of Fe<sub>6</sub>Nd<sub>4</sub>. The obtained slag concentrate based on the oxides of rare earth elements is suitable for further pyrometallurgical or hydrometallurgical treatment in order to obtain rare earth elements.

**Keywords:** recycling; smelting; oxidation; rare earth elements; magnets



**Citation:** Chung, H.; Stopic, S.; Emil-Kaya, E.; Gürmen, S.; Friedrich, B. Recovery of Rare Earth Elements from Spent NdFeB-Magnets: Separation of Iron through Reductive Smelting of the Oxidized Material (Second Part). *Metals* **2022**, *12*, 1615. <https://doi.org/10.3390/met12101615>

Academic Editors: Antonije Onjia and Fernando Castro

Received: 6 August 2022

Accepted: 25 September 2022

Published: 27 September 2022

**Publisher's Note:** MDPI stays neutral with regard to jurisdictional claims in published maps and institutional affiliations.



**Copyright:** © 2022 by the authors. Licensee MDPI, Basel, Switzerland. This article is an open access article distributed under the terms and conditions of the Creative Commons Attribution (CC BY) license (<https://creativecommons.org/licenses/by/4.0/>).

## 1. Introduction

In the previous study, the problem of separating iron from REE is present in the hydrometallurgical treatment of NdFeB spent magnets, so the application of pyrometallurgical treatment is being considered. The aim of the first part was to study the oxidation of spent NdFeB-magnets as preparation for the second phase-reductive smelting process [1]. The obtained results have confirmed that maximal total oxidation of spent NdFeB-magnets was 90% obtained at 1000 °C in 45 min. Selective oxidation of REE from Fe and B is not possible in the interval between 500 and 1000 °C.

XRD analysis was conducted on both phases, and results showed that the rare earth elements are in the form of metal oxide, such as Dy<sub>2</sub>O<sub>3</sub>, Pr<sub>2</sub>O<sub>3</sub>, NdFeO<sub>3</sub>, Nd<sub>2</sub>O<sub>3</sub>, and NdFeO<sub>3</sub>. Boron is present in the form of NdBO<sub>3</sub> and FeB<sub>2</sub>. Iron is oxidized in the form of Fe<sub>2</sub>O<sub>3</sub> and Fe<sub>3</sub>O<sub>4</sub>. Further, 5.11% of the iron is in the form of α-iron and iron oxide. In order to separate rare earth elements from Fe and B, additional reduction of the oxidized material is necessary in the next step.

REE are known as 'industrial vitamins', obtaining significant attention worldwide. Currently, REE are vital components of many modern technologies, including electric and conventional cars, computers and smartphones, renewable energy infrastructure, and phosphor light [1].

Yang et al. [2] presented a critical review of REE Recovery from End-of-Life NdFeB permanent magnet scrap, providing the list of efficient technologies that will be developed and included in practice. The research strategy used in this work is presented in Figure 1, as previously mentioned by Kruse et al. [3,4].

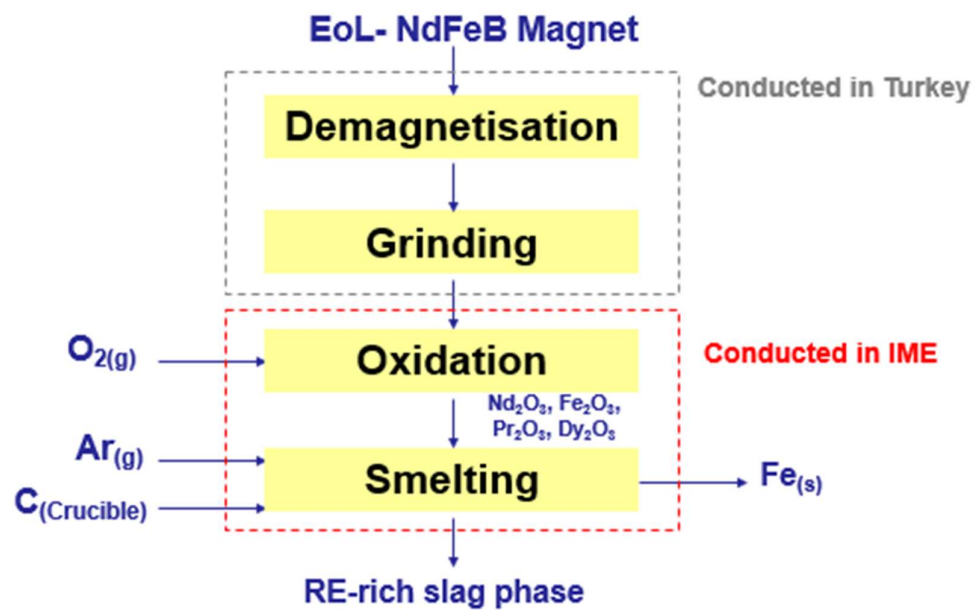


**Figure 1.** Proposed strategy for study in this work.

The first step of the work converts the initial magnet sample into a high oxygen potential component by oxidation within a muffle furnace. The unconventional way of converting the magnets into an oxide form allows the utilization of the difference in oxygen affinity between the REE and Fe phases. By placing the oxidized materials in a carbon crucible, the contact carbon could be used to reduce the iron oxides while leaving the REE in oxide form. The control of the oxygen potential within the input materials allows the effective carbothermic reduction without having the need to precisely control  $CO/CO_2$  ratio or the carbon content within the material, since both of which would be in oversupply for the reduction process.

The extraction of Nd from waste Nd–Fe–B alloys was studied by the glass slag method [5], microwave-assisted carbothermic reduction [6], and through the interaction of rare earth element neodymium, iron, and arsenic at 900 °C [7] confirming that separation of iron is possible during the pyrometallurgical method. In comparison to the pyrometallurgical method, the hydrometallurgical method offers a separation of iron during precipitation and acidic baking [8–20]. Orefice [21] mentioned selective roasting of Nd–Fe–B permanent magnets as an important pretreatment step for intensified leaching with an ionic liquid.

Efstratiadis [22] offered a detailed review about sustainable recovery, recycling of critical metals and rare earth elements from waste electric and electronic equipment (circuits, solar, wind), and their reusability in additive manufacturing applications.

The aim of the current research is to use the previously mentioned findings in order to recover REEs by means of pyrometallurgical smelting, separating the magnets into a metal phase and rare earth oxide (REO) rich slag.

## 2. Materials and Methods

Spent magnets from the company Miknatis Ar-Ge in Istanbul, Turkey, are obtained and conditioned prior to the experiment phase. These were first demagnetized at 350 °C for 30 min and milled into magnet powders. The samples were thermally treated by oxidizing them in air and then smelted in a vacuum induction furnace (MiniVIM/Heraeus, Hanau, Germany) under an argon atmosphere. The phase analysis of the magnet powders was investigated by XRD (Bruker D8 Advance, Karlsruhe, Germany) equipment with a standard Cu wavelength of 1.5406 Å. Chemical analysis of the leachate obtained after the total dissolution of spent NdFeB magnets was conducted using ICP-OES (Spectro Arcos, SPECTRO Analytical Instruments Gmb, Kleve, Germany). Dynamic particle size analysis was conducted by a dynamic particle analyzer (Sympatec QuickPick Oasis with an M5

lense, software PAQXOS 4.1, (Sympatec GmbH, Clausthal Zellerfeld, Germany). The SEM analysis was performed on the JSM 7000F by JEOL (construction year 2006, JEOL Ltd., Tokyo, Japan) and EDX analysis using the Octane Plus-A by Ametek-EDAX construction year 2015, AMETEK Inc., Berwyn, PA, USA), with software Genesis V 6.53 by Ametek-EDAX., Berwyn, PA, USA). The oxidation experiments were performed in a small tubular Furnace, Thermostar, Aachen [1].

The chemical analysis of NdFeB-powder was (%): 21.7 REE, 73.8 Fe, 0.66 B, and 0.0006 Ni, as shown in Table 1.

**Table 1.** Chemical analysis of powder.

Sample NdFeB (%)	Nd	Ni	Fe	B	Pr	Dy
Weight (%)	15.9	0.0006	73.8	0.662	5.6	0.201

As shown in Table 2, the quantitative XRD-analysis of NdFeB-powder found next composition (%) 87.19 Nd<sub>2</sub>FeB<sub>14</sub>, 3.05 Pr<sub>2</sub>FeB<sub>14</sub>, 4.26 FeB<sub>5</sub>, 2.04 DyFe<sub>2</sub> and 2.46 DyFe<sub>5</sub>.

**Table 2.** Rietveld XRD- quantitative analysis of NdFeB-magnets.

Phase	DyFe <sub>2</sub>	DyFe <sub>5</sub>	FeB <sub>5</sub>	Nd <sub>2</sub> Fe <sub>14</sub> B	Pr <sub>2</sub> Fe <sub>14</sub> B
Weight%	2.46	3.04	4.26	87.19	3.04

Particle size analysis of powder revealed 50% particles about 39.85 µm. The smallest fraction amounts were 7.35 µm in comparison to the largest fraction of 90.40 µm, as shown in Table 3.

**Table 3.** Particle size analysis of NdFeB-powder after demagnetizing, grinding, and sieving.

Samples (µm)	X <sub>30</sub>	X <sub>50</sub>	X <sub>90</sub>
NdFeB	7.35	39.85	90.40

The oxidation of 1 kg of spent NdFeB magnets was performed at 1000 °C in a time of 2 h in order to prepare the sample for reductive smelting in a graphite crucible. The actual oxidation of the bulk magnet samples shows lesser mass change than the recorded results from DTA/TG, i.e., incomplete oxidation. The final mass change contributed by the oxidation was 27.2 wt.%, while the corresponding degree of oxidation of the mass sample was 78%. A qualitative X-ray diffraction analysis (XRD analysis) was conducted on the oxidized sample to determine the formed oxide phases and the influence of temperature on the formation of different phases.

According to the XRD analysis, the oxidized material does not only consist entirely of metal oxides but also some metallic phases. Through oxidation, the majority of Nd<sub>2</sub>Fe<sub>14</sub>B is decomposed to form Fe-oxides, Nd<sub>2</sub>O<sub>3</sub>, and NdFeO<sub>3</sub>, as shown in Table 4.

**Table 4.** XRD analysis of oxidized NdFeB sample.

Phase	Dy <sub>2</sub> O <sub>3</sub>	FeB <sub>2</sub>	Fe <sub>2</sub> O <sub>3</sub>	Fe <sub>3</sub> O <sub>4</sub>	NdBO <sub>3</sub>	NdFeO <sub>3</sub>	Nd <sub>2</sub> O <sub>3</sub>	α-Fe	Pr <sub>2</sub> O <sub>3</sub>
Weight%	1.28	1.75	53.41	10.37	10.01	16.45	0.45	5.22	1.07

The obtained quantitative analysis in (wt.%) has shown 53.41 Fe<sub>2</sub>O<sub>3</sub>, 10.37 Fe<sub>3</sub>O<sub>4</sub>; 16.45 NdFeO<sub>3</sub>; 0.45 Nd<sub>2</sub>O<sub>3</sub>, 1.28 Dy<sub>2</sub>O<sub>3</sub>, 1.07 Pr<sub>2</sub>O<sub>3</sub>, and 5.22 α-Fe. The presence of boron in 10.01% NdBO<sub>3</sub> is in agreement in comparison to 0.668% present boron in structure. It is assumed that a small amount of NhdBO<sub>3</sub> has covered the high expected Pr<sub>2</sub>O<sub>3</sub> or PrFeO<sub>3</sub>, which is not detected in the structure. A hypothesis for this observation is the entrapped particles within the bulk phase, such as NdBO<sub>3</sub> or NdFeO<sub>3</sub>, which caused the non-detection under the XRD analysis. A second possibility was that the actual thermodynamic situation

within the materials does not favor the formation of  $\text{PrFeO}_3$  due to the lower chemical activity of Pr compounds and statistical occurrences of oxygen contact with such compounds. The presence of  $\alpha\text{-Fe}$  is not expected in oxidized structure, but it will be separated during reductive smelting at higher temperatures.

## 2.1. Reductive Smelting of the Oxidized Sample

### 2.1.1. Thermochemical Analysis of Reductive Smelting

A ternary phase diagram with liquidus temperature projection of the Nd-Fe-B system as obtained from the simulation software FactSage 8.0 (GTT-Technologies, Aachen, Germany) is illustrated in Figure 2. Since the sample used in this study contains traces of several other elements adding up to more than 5 wt.%, the exact melting temperature of the system could not be identified accurately; however, an approximation could be drawn based on this diagram: at compositions of 69.7 to 73.8 wt.% Fe and 15.9 to 18.7 wt.% Nd (orange circle in the diagram), the melting temperature lies in ranges of 1400–1500 °C.

Within the same software under the *Equilib* function, the melting point is approximated by taking the temperature at which the total mixture is in a molten state.

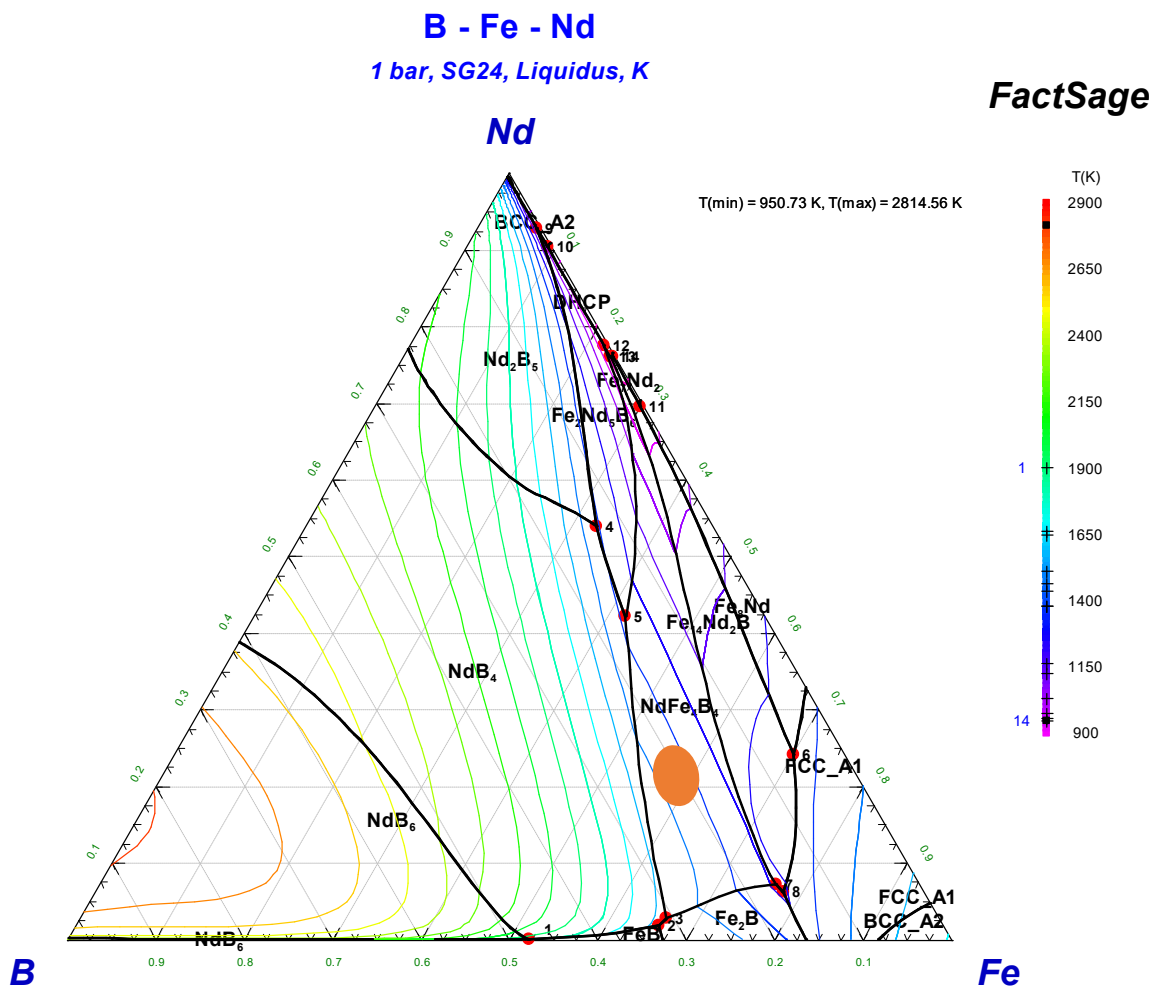


**Figure 2.** Ternary phase diagram of Nd-Fe-B system with liquidus temperature projection.

The results are included in Figure 3, with the melting temperature being around 1400 °C. The melting temperature was taken at the temperature from which no further phases other than the liquid phase form. In the mass-temperature plot, only the main phases of mass larger than 10 g are included (compare Table 5), while the presence of other phases is not included as the amount is insignificant. The starting material for thermochemical

calculation is the initial composition of NdFeB-spent magnets, which is shown in Figure 2. The content of the four theoretical phases is stated in Table 5.

**Table 5.** List of (theoretical) main phase present near the melting point.

Phase	Component Present
hR <sub>57</sub>	mixture of Dy <sub>2</sub> Fe <sub>17</sub> , Nd <sub>2</sub> Fe <sub>17</sub> , Pr <sub>2</sub> Fe <sub>17</sub>
Liqu#1	liquid state mixture of all elements
Fe_Liqu#1	Fe-portion of the total liquid phase
A <sub>1</sub> #1	γ-Fe (FCC)

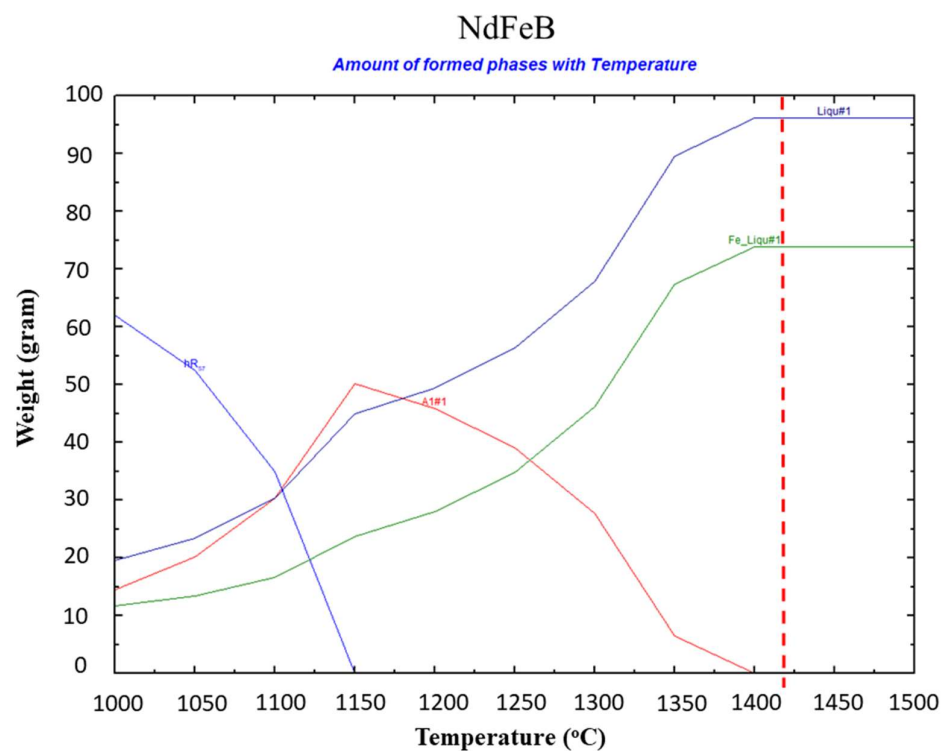


**Figure 3.** Number of formed phases with a temperature of NdFeB from 1000–1500 °C.

Considering the thermodynamics of metal oxidation, a widely used tool in the metallurgy field is the Richardson–Ellingham diagram, which plots the standard free enthalpies of formation for the reduction of metal oxide to metals over temperature. The standard free enthalpies of formation in equilibrium can be calculated according to Equation (1), under the assumption that the temperature dependence of  $\Delta H$  and  $\Delta S$  is negligible. Based on this equation, a Richardson–Ellingham diagram as adapted from Kruse et al. [3,4] is shown in Figure 4.

$$\Delta G^0 = \Delta H^0 - T\Delta S^0 = -RT \ln(k) \quad (1)$$

A pre-requisite for a reduction reaction to take place, according to the Richardson–Ellingham diagram, is that the metal must have a lower affinity for oxygen than the reducing agent. In other words, the  $\Delta G^0$  line of the target metal has to be above the  $\Delta G^0$  line of the reducing agent. Due to a lack of thermodynamic data, a simplification is adapted here, where individual activities of each element in the multi-component system are not considered. The Richardson–Ellingham diagram shows that REEs have the highest affinity for oxygen in pure substances. Unlike REEs, iron has a much higher oxygen affinity and can be reduced by several elements, including carbon and aluminum.

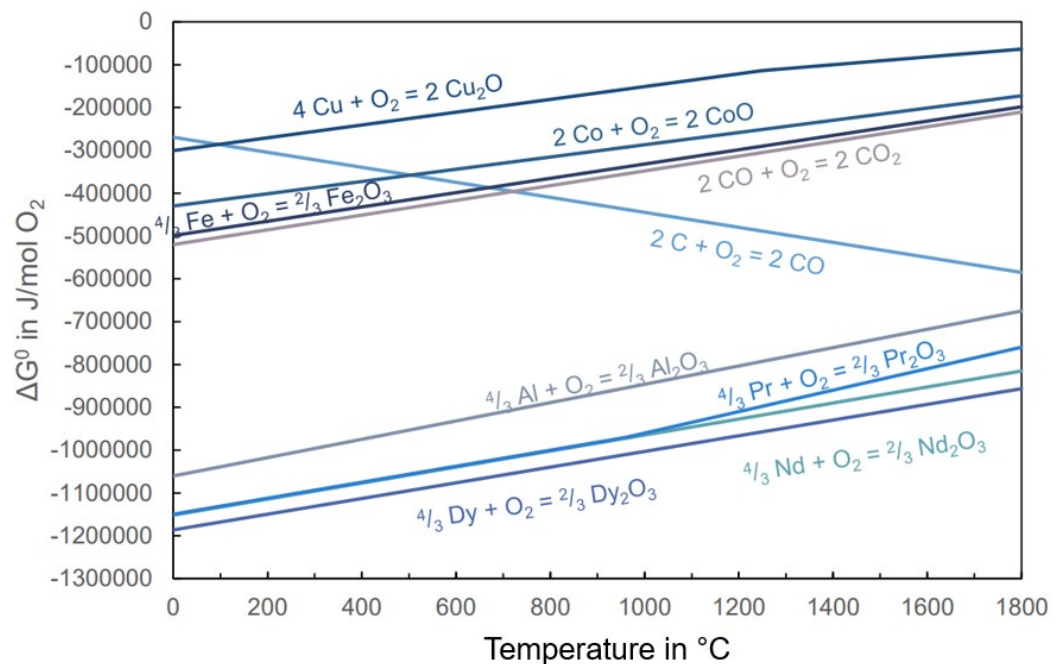
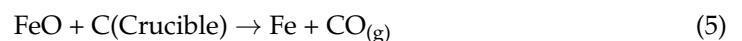
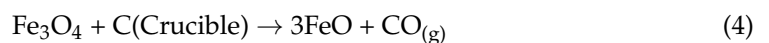
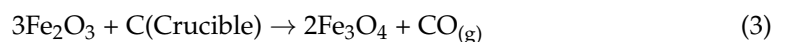
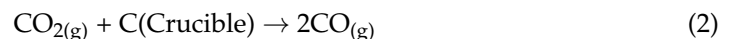


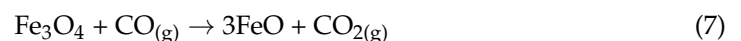
**Figure 4.** Richardson–Ellingham diagram for selected metals.

Under the presence of carbon, it can be seen that from 700 °C onwards, a carbothermic reduction on iron is easily feasible. In addition to that, it is impossible to reduce REE-oxides ( $\text{Nd}_2\text{O}_3$ ,  $\text{Dy}_2\text{O}_3$ , and  $\text{Pr}_2\text{O}_3$ ) into elemental REEs using carbon even up to a temperature of 1800 °C. This proposes an efficient separation method for the REEs and Fe from the magnet powders [5]. In the present work, a clay graphite crucible was used as the source of over stoichiometric carbon supply in the form of contact material.

The reduction mechanism for iron formation from iron oxide was well established within the steel and iron-making industry and will not be explained in detail here. The carbothermic reduction can be separated into direct reduction between iron oxides and carbons and indirect reduction involving the removal of oxygen from iron oxides by carbon monoxides [6]. Further, part of the direct reduction is the Boudouard reaction, which produces carbon monoxides by reacting carbon and carbon dioxides. The equations are listed in Equations (2)–(8) below:



#### Direct Reductions



#### 2.1.2. Experimental Reductive Smelting in an Induction Furnace

The oxidized magnets samples were then smelted in 3 experiments at varying parameters. The first experiment used 100 g of magnet powders with holding times of 10 min; this was proven to be excessive as some of the content overflowed the crucible with the dimension of 7 cm depth and 4 cm diameter opening. Further experiments were then conducted

with 60 g of input materials. The targeted holding temperature for the experiments varies between 1350 °C (1623.15 K) and 1500 °C (1773.15 K). A list of conducted experiments is shown in Table 6.

**Table 6.** Completed smelting experiment in argon.

Trials	Materials	Mass (g)	Temperature (°C)
V1	NdFeB	100	1500
V2	NdFeB	60	1400
V3	NdFeB	60	1350

The smelting was conducted inside a clay graphite crucible for its high-temperature resistance and simultaneous ability to supply carbon for the reduction. This was placed within a sand bed and topped with fiberglass wool for heat insulation.

As shown in Figure 5, two thermocouples were used to monitor the temperature within the crucible and outside of the crucible. The experiments were conducted under a low-pressure argon gas atmosphere of 80 mbar. Selected slag samples and metal samples were ground into powders and sent for ICP-OES analysis, while one sample was selected for qualitative XRD analysis.

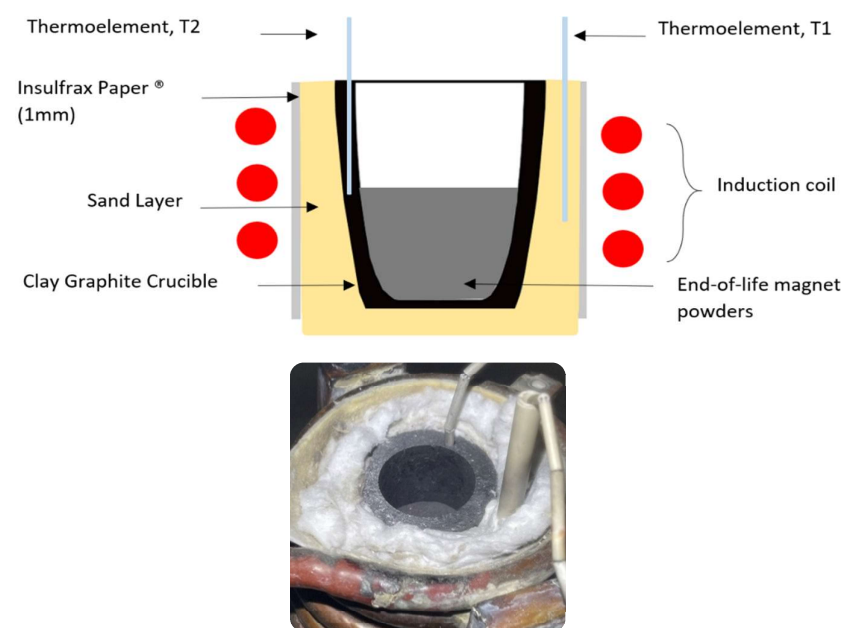


**Figure 5.** Experimental setup of graphite crucible in an induction furnace.

### 3. Results

As shown in Figure 6, in all 3 experiments, an obvious separation between a metallic phase and a slag phase can be seen. In addition to that, a corroded crucible wall was observed. This could be explained by the carbon supply from the clay graphite crucible for the carbothermic reduction of the iron oxides in the input materials.

The chemical composition of the metal phase from the NdFeB sample is shown in Figures 7 and 8, and the main component is iron for both samples, with traces of several other elements, such as the REEs and boron. Comparing the initial concentrations of the pre-oxidized materials with 73.8 wt.% Fe in NdFeB, the increase in Fe content confirms that the methodology of using carbothermic reduction with clay graphite crucible as the source of carbon supply is viable.

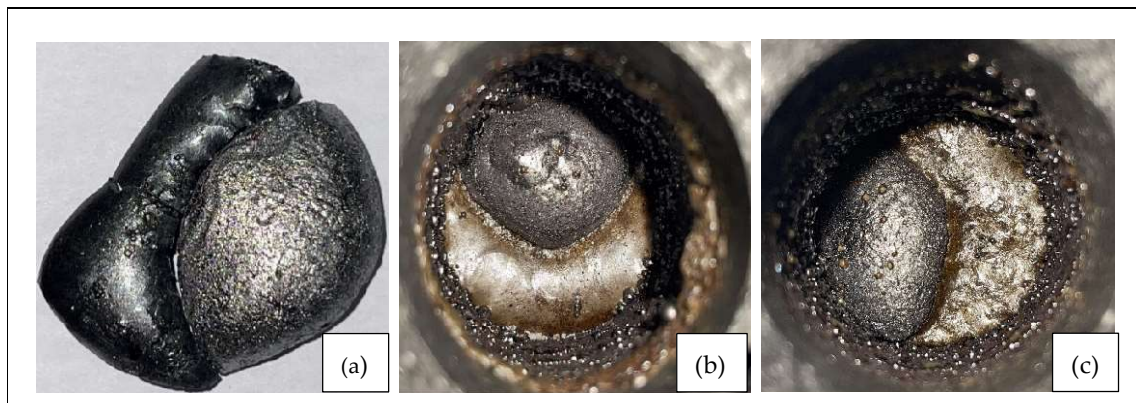


Figure 6. Post experimental observations: Metal Slag separation in V1 (a), V2 (b), V3 (c).

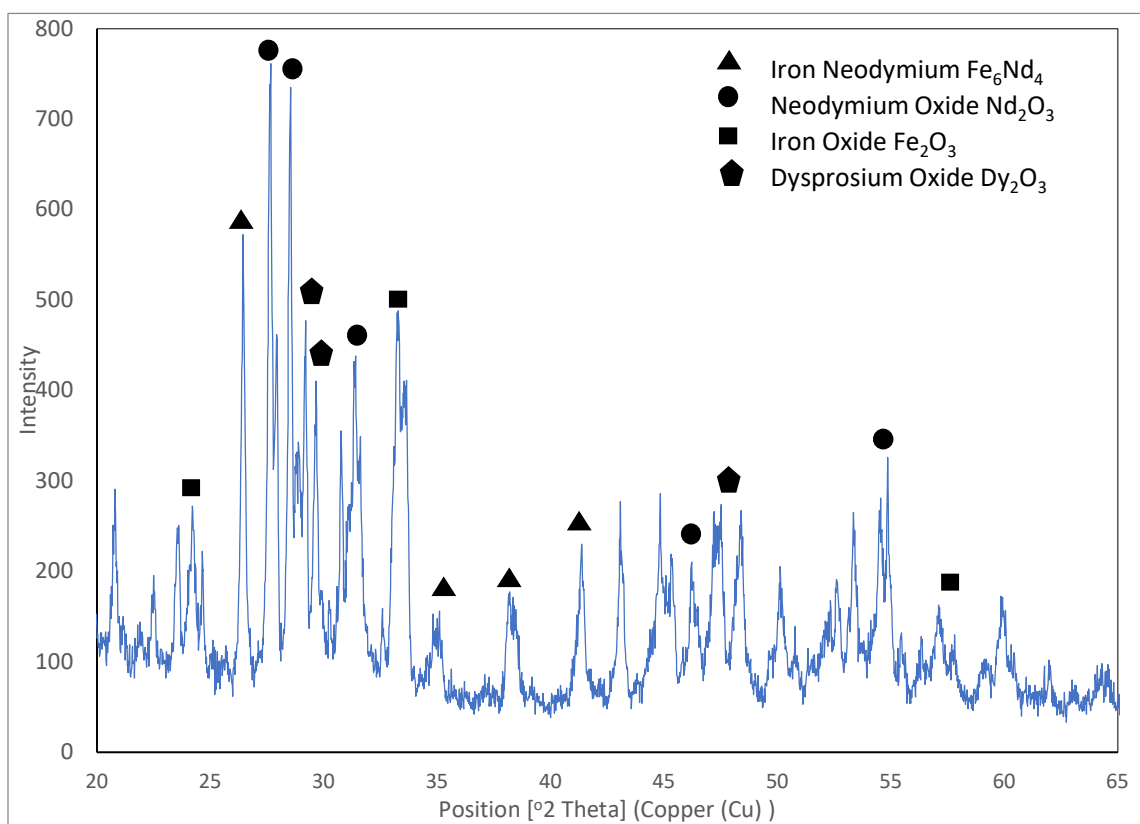
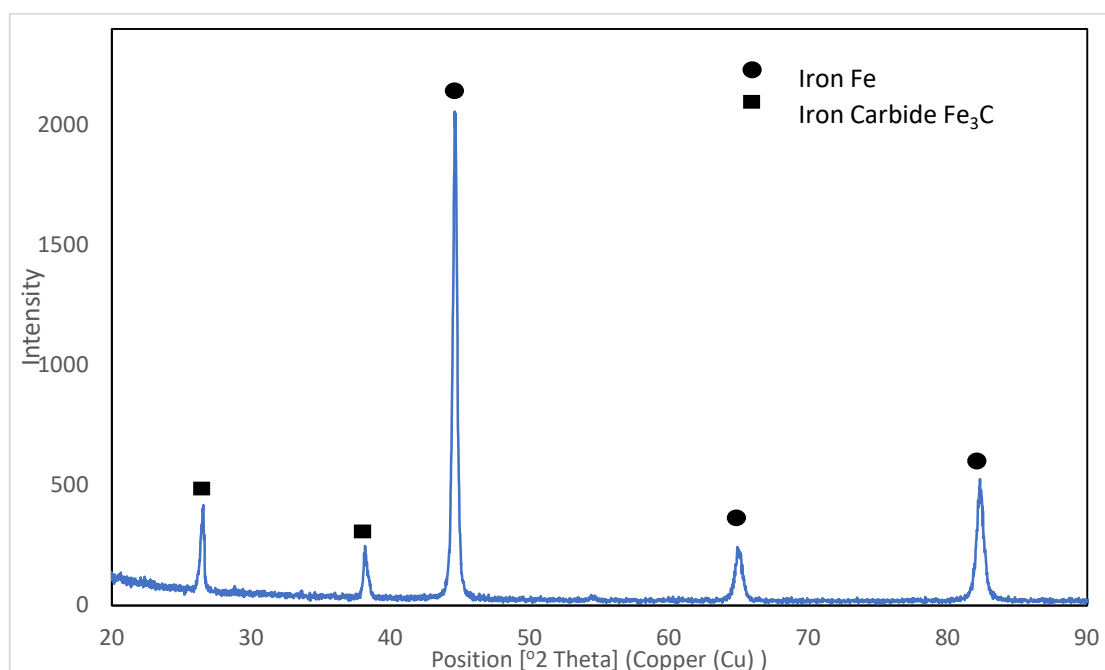


Figure 7. XRD analysis of slag phase from experiment V3.

Fe-separation represents the mechanical separation of metallic iron from the created slag. Generally, slag was separated by metallic iron from the formed mixture. Based on Table 7, the separation efficiency in the metallic phase amounts of 98.1%, 98.9%, and 97.5% for Nd, Pr, and Dy at 1500 °C, respectively. The excellent separation efficiency is also confirmed in V2 at 1400 °C. Separation efficiency in the metallic phase amounts of 96.9%, 97.2%, and 95.8% for Nd, Pr, and Dy at 1400 °C, respectively. The reduced efficiency of the REE-separation during reductive smelting is a consequence of the reduction of the melting temperature from 1500 °C to 1400 °C.



**Figure 8.** XRD analysis of metallic phase from experiment V3.

**Table 7.** ICP-OES analysis of smelting product (%).

Samples/Elements	Nd	Fe	B	Pr	Dy
V1 Metal	0.312	82.9	0.0876	0.0607	0.005
V1 Slag	37.34	1.78	1.642	9.43	0.703
V2 Metal	0.47	92.2	0.14	0.108	0.0084
V2 Slag	32.2	0.603	2.084	10.8	0.43

A similar analysis was conducted on the slag phase, and the results are shown in Figures 9 and 10. This analysis shows the elemental REEs as well as traces of several other elements, such as iron and boron, present in the slag phase after melting. The presence of boron was explained by Kruse et al. [3,4] to be a form of  $B_2O_3$ . The nearly 2-fold increase in REEs content in the slags corresponds to the initial hypothesis that REE-oxides will not be carbothermally reduced might be confirmed. Comparing the initial concentration of the pre-oxidized materials, the method of oxidizing and eventual smelting with carbothermic reduction resulted in the production of RE concentrates.

The resulting concentrate contains 47.47% of rare earth instead of the original 21.7%, which confirms a good choice of strategy for separating elements, as shown in Figure 9. In the experiment at 1400 °C, the obtained concentrate contains about 45% rare earth elements. The separation efficiency for iron amounts of 2.5% and 0.8% at 1500 °C and 1400 °C, respectively. Boron is presented not only in the metallic phase, but also in slag concentrate. An increase in smelting reductive temperature from 1400 °C to 1500 °C leads to a decrease in boron content from 1.642 to 0.14%, as shown in Figure 10.

The results of the qualitative XRD analysis of the metallic and slag phase from experiment V3 are shown in Figures 7 and 8.

The slag phase showed corresponding RE-oxides (Nd and Dy), leftover iron oxides, and a mixture compound of  $Fe_6Nd_4$ , which typically forms at a temperature above 1000 °C [7]. Despite the fact that there is a high amount of Pr compared to Dy in the input materials, no  $Pr_2O_3$  was detected in the sample and this could be a source of error from the chosen analytical method. The XRD analysis, however, confirmed that the slag consists of mainly oxides, and the methodology of this work to produce RE-rich slag can be proven to

be viable. As shown in Figure 8, the metallic phase consists mainly of iron and iron carbide. The presence of the carbide phase can be explained by a continuous dissolving of carbon from the crucible into the molten iron throughout the smelting process. The SEM-EDS mapping of metal phase from V3 is shown in Figure 9:

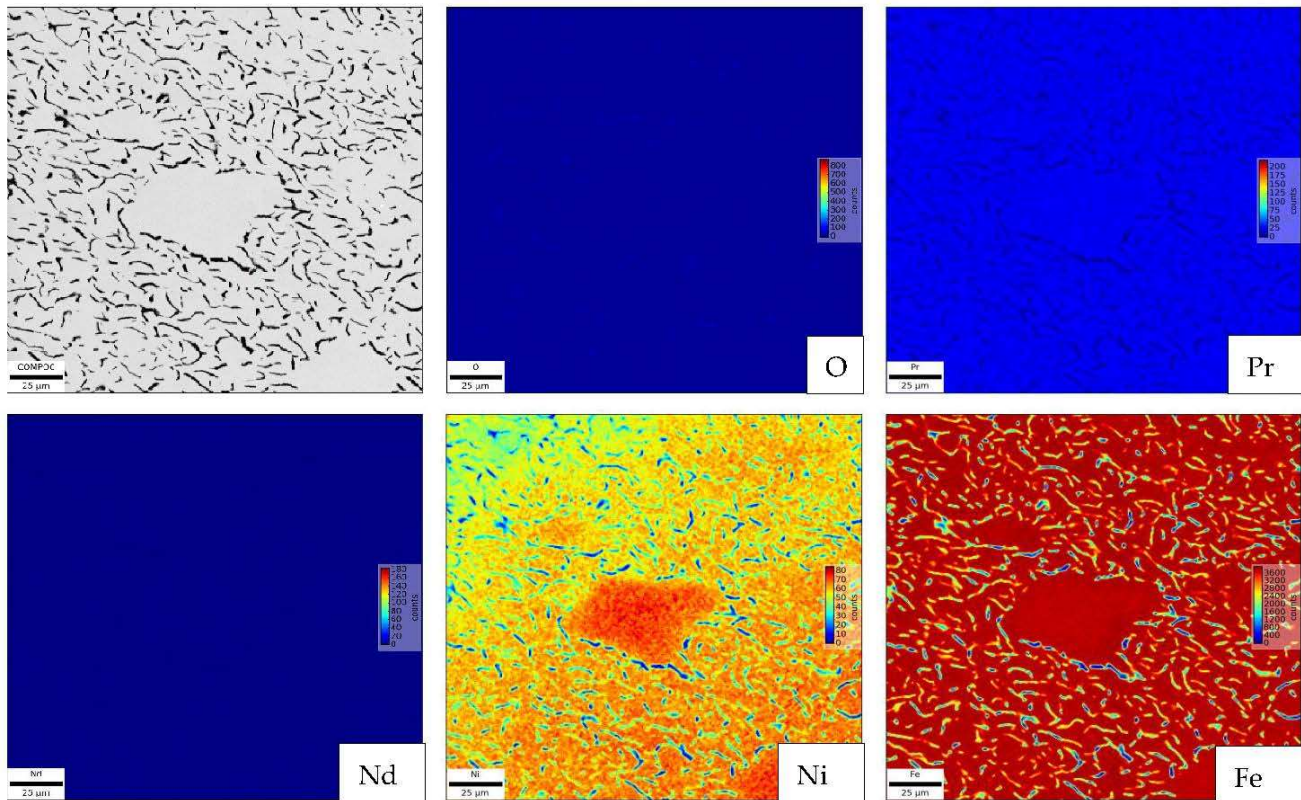


**Figure 9.** SEM-EDS mapping of metal phase from V3.

The metallic phase extracted from the crucible consists mainly of Fe with large amounts of Ni. Oxygen and Nd are close to zero counts and Pr at very low counts, which confirms the purity of the metallic phase. Although the mapping results did not include carbon, the presence of carbon should not be disregarded. The dark dendrite-like regions with low to no counts of other elements should correspond to carbon, as there was an over-stoichiometric carbon supply from the clay graphite crucible in the experimental study conducted. A direct recycling of this steel or metallic Fe obtained from the carbothermic reduction in other applications could be impractical due to the heterogeneous impurities in the phases that vary from each experiment.

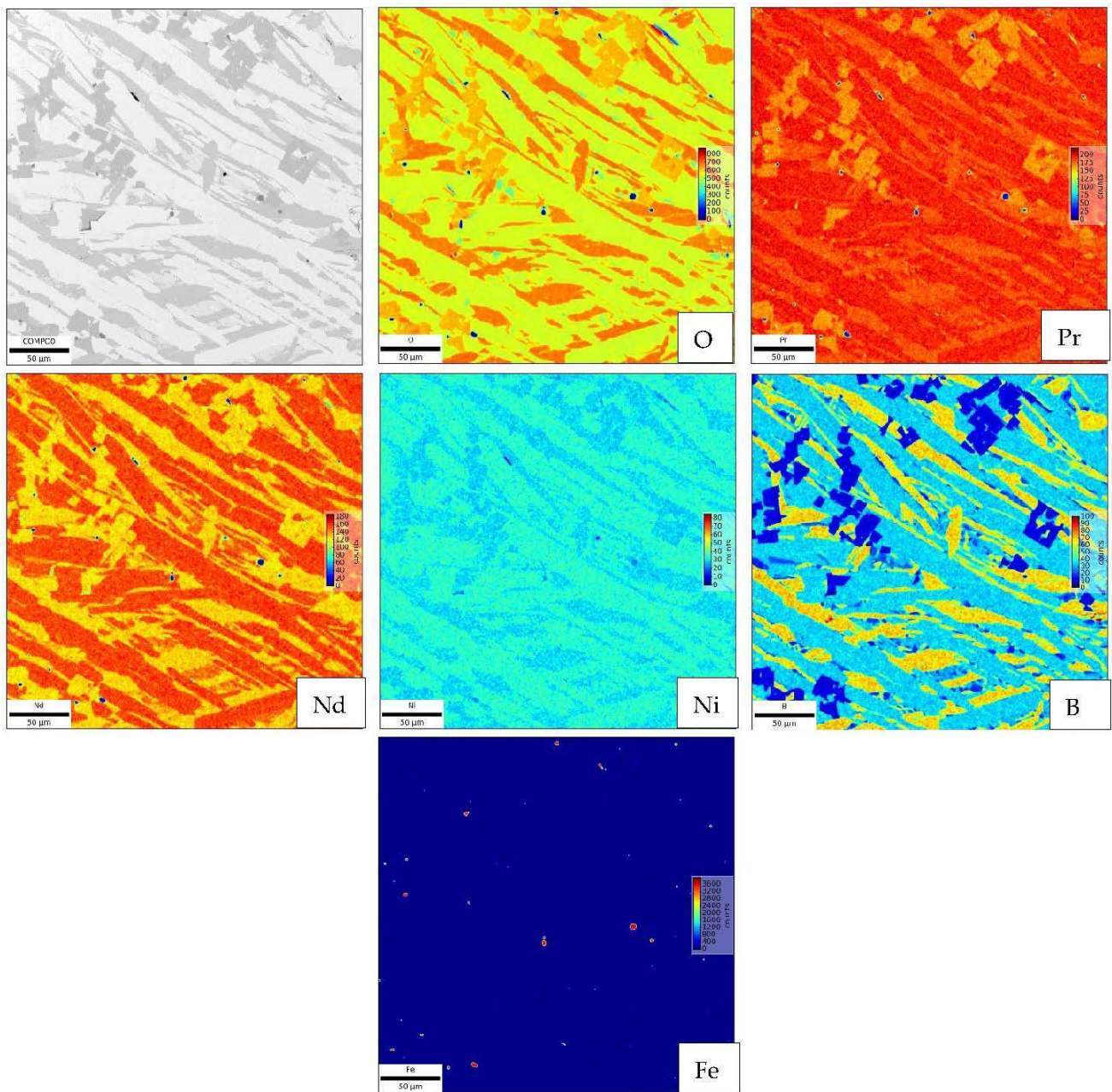


Figure 10. SEM-EDS mapping of slag phase from V3.

#### 4. Discussion

The slag phase extracted from the crucible consists mainly of oxides of Pr, Nd, and B. The distribution of boron upon smelting can be seen based on these images, that it forms oxides that are enriched in the slag phase. Several extremely high counts of Fe spots can be observed in the image as well. There are two possibilities to explain this observation, which are droplets lost during metal slag separation that is supported by induction stirring. A second conjecture is such that these Fe are already present in the matrix prior to smelting and could not be separated since the oxidation process does indeed produce alpha-Fe according to XRD analysis.

The results from these experiments have verified the viability of the proposed method on the first test. Although repeated experiments have not been conducted yet, the results showed a very optimistic starting point for further experimental work. A direct implementation of this method on an industrial scale, however, does not promise a desirable outcome as there are still many optimizing possibilities, such as the oxidation condition from the first

part, the smelting parameters, and the carbon supply from this current work. An upscaling should be planned to verify not only the metallurgical aspects but also the engineering aspects of the proposed method in order for this to be implemented in commercial activities. Based on the current experiment results, upscaling should first focus on the carbon supply for the carbothermic reduction, as this work uses the carbon from the crucible itself. Relying solely on the supply of carbon from the crucible in a larger-scale smelting experiment could result in leakage or holes in the crucible wall owing to the corrosion, i.e., carbon supply, which eventually causes damage to the furnace. Furthermore, engineering simulations and studies could be conducted to connect the oxidation part and the reducing part, which could potentially lower the energy consumption by using the already heated up materials directly after the oxidation. The possibility of scaling and implementation of reductive smelting is very high, which is the subject of our future work. The final part of this work is metal winning during molten salt electrolysis using the prepared slag concentrate based on mixed oxides of rare earth elements. These results shall be mentioned in the third part of this study.

## 5. Conclusions

In this study, a research methodology of recycling end-of-life NdFeB magnets used by S.Kruse et al. [3,4] is validated and improved during reductive smelting. The aim of the work was to recover REEs by means of pyrometallurgical smelting, separating the magnets into a metallic phase and an RE-oxide-rich slag phase. This aim was achieved and confirmed by experimental trials conducted during the study.

From the products of smelting, the metal phase showed a maximum Fe content of 92.3 wt.%, while the slag phase showed a maximum total REE (Nd, Pr, and Dy) content of 47.47 wt.%, both at a smelting temperature of 1500 °C. The separation efficiency of rare earth elements between 1400 °C and 1500 °C amounts of 96.9–98.1, 97.2–98.9, and 95.8–97.5 for Nd, Pr, and Dy. An increase in temperature from 1400 °C to 1500 °C not only increases the separation efficiency of rare earth elements but also decreases the content of boron from 2.8 to 1.64 in produced slag.

ICE-OES and XRD analysis were conducted on both phases, and results showed that the metal phase consists mainly of Fe and Fe<sub>3</sub>C while the slag phase consists of the RE-oxides, leftover Fe<sub>2</sub>O<sub>3</sub>, and a mixture of Fe<sub>6</sub>Nd<sub>4</sub>.

This work investigated process optimization, the recovery of the RE-oxide-rich slag, and the identification of limits to the carbothermic reduction. The results concluded here could be applied for further laboratory scaled studies and aids the development trend towards a sustainable economy. The following treatment of the RE-oxide-rich slag is planned by molten salt electrolysis or hydrometallurgical route.

**Author Contributions:** Conceptualization, S.S. and E.E.-K.; methodology, H.C.; software, H.C.; validation, S.S., E.E.-K. and H.C.; formal analysis, S.G.; investigation, H.C.; resources, S.S.; data curation, E.E.-K.; writing—original draft preparation, H.C.; writing—review and editing, S.S.; visualization, H.C.; supervision, S.G.; project administration, H.C.; funding acquisition, S.G. and B.F. All authors have read and agreed to the published version of the manuscript.

**Funding:** This research was funded by the Federal Ministry for Economic Affairs and Climate Action, grant number 287 EN, and The Scientific of Technological Research Council of Turkey under grant agreement 120N33. The APC was funded by the project “Sustainable recovery of rare earth elements (Nd, Pr, Dy) from spent magnets”.

**Data Availability Statement:** Not applicable.

**Conflicts of Interest:** The authors declare no conflict of interest.

## References

1. Stopic, S.; Polat, B.; Chung, H.; Smiljanic, S.; Elif-Kaya, E.; Gürmen, S.; Friedrich, B. Recovery of Rare Earth Elements from spent NdFeB-magnets—Reductive Smelting of the oxidized material (First Part). *Metals* **2021**, *11*, 716.
2. Yang, Y.; Walton, A.; Sheridan, R.; Güth, K.; Gauß, R.; Gutfleisch, O.; Buchert, M.; Steenari, B.-M.; van Gerven, T.; Jones, P.T.; et al. REE Recovery from End-of-Life NdFeB Permanent Magnet Scrap: A critical Review. *J. Sustain. Metall.* **2017**, *3*, 122–149.
3. Kruse, S.; Raulf, K.; Pretz, T.; Friedrich, B. Influencing Factors on the Melting Characteristics of NdFeB-Based Production Wastes for the Recovery of Rare Earth Compounds. *J. Sustain. Metall.* **2017**, *3*, 168–178. [[CrossRef](#)]
4. Kruse, S.; Raulf, K.; Trentmann, A.; Pretz, T.; Friedrich, B. Processing of Grinding Slurries Arising from NdFeB Magnet Production. *Chem. Ing. Tech.* **2015**, *87*, 1589–1598. [[CrossRef](#)]
5. Saito, T.; Sato, H.; Ozava, S.; Yu, J.; Montegi, T. The extraction of Nd from waste Nd–Fe–B alloys by the glass slag method. *J. Alloys Compd.* **2003**, *353*, 189–193. [[CrossRef](#)]
6. Tanvar, H.; Dhawan, N. Microwave-Assisted Carbothermic Reduction of Discarded Rare Earth Magnets for Recovery of Neodymium and Iron Values. *JOM* **2021**, *73*, 54–62. [[CrossRef](#)]
7. Xie, W.; Huang, R.; Zhang, J.; Li, W.; Yang, Y. Study on the interaction of rare earth element neodymium, iron and arsenic at 1173 K. *Gongneng Cailiao/J. Funct. Mater.* **2018**, *49*, 1134–1138. [[CrossRef](#)]
8. Peelman, S.; Kooijman, D.; Sietsma, J.; Yang, Y. Hydrometallurgical Recovery of Rare Earth Elements from Mine Tailings and WEEE. *J. Sustain. Metall.* **2018**, *4*, 367–377. [[CrossRef](#)]
9. Peelman, S.; Sietsma, J.; Yang, Y. Recovery of Neodymium as (Na, Nd)(SO<sub>4</sub>)<sub>2</sub> from the Ferrous Fraction of a General WEEE Shredder Stream. *J. Sustain. Metall.* **2018**, *4*, 276–287. [[CrossRef](#)]
10. Ma, Y.; Stopic, S.; Gronen, L.; Milivojevic, M.; Obradovic, S.; Friedrich, B. Neural Network Modeling for the Extraction of Rare Earth Elements from Eudialyte Concentrate by Dry Digestion and Leaching. *Metals* **2018**, *8*, 267. [[CrossRef](#)]
11. Yun, Y.; Stopic, S.; Friedrich, B. Valorization of Rare Earth Elements from a Steenstrupine Concentrate via a Combined Hydrometallurgical and Pyrometallurgical Method. *Metals* **2020**, *10*, 248.
12. Kumari, A.; Sinha, M.; Pramanik, S.; Sahu, S. Recovery of rare earths from spent NdFeB magnets of wind turbine: Leaching and kinetic aspects. *Waste Manag.* **2018**, *75*, 486–498. [[CrossRef](#)]
13. Ma, Y.; Stopić, S.; Friedrich, B. Hydrometallurgical Treatment of an Eudialyte Concentrate for Preparation of Rare Earth Carbonate. *Johns. Matthey Technol. Rev.* **2019**, *63*, 2–13. [[CrossRef](#)]
14. Stopic, S.; Friedrich, B. Advances in Understanding of the Application of Unit Operations in metallurgy of rare earth elements. *Metals* **2021**, *11*, 978. [[CrossRef](#)]
15. Umweltbundesamt. Seltene Erden in Permanentmagneten. In *Für Mensch und Umwelt-Factsheet*; Umweltbundesamt: Dessau-Roßlau, Germany, 2019; pp. 1–10.
16. Stopic, S.; Friedrich, B. Leaching of rare earth elements from bastnasite ore: Second part. *Mil. Tech. Cour.* **2019**, *67*, 241–254. [[CrossRef](#)]
17. Stopic, S.; Friedrich, B. Leaching of rare earth elements from bastnasite ore (third part). *Mil. Tech. Cour.* **2019**, *67*, 561–572. [[CrossRef](#)]
18. Uysal, E.; Al, S.; Stopic, S.; Gürmen, S.; Friedrich, B.; Kaya, E.E. Hydrometallurgical recycling of waste NdFeB magnets: Design of experiment, optimisation of low concentrations of sulphuric acid leaching and process analysis. *Can. Metall. Q.* **2022**, *61*, 1–12. [[CrossRef](#)]
19. Kaya, E.; Kaya, O.; Stopic, S.; Gürmen, S.; Friedrich, B. NdFeB Magnets recycling process: An alternative method to produce mixed rare earth oxide from scrap NdFeB magnets. *Metals* **2021**, *11*, 716. [[CrossRef](#)]
20. Klemettinen, A.; Zak, A.; Chojnacka, I.; Matuska, S.; Lesniewicz, A.; Welna, M.; Adamsky, Z.; Klemettinen, L.; Rycerz, L. Leaching of Rare Earth Elements from NdFeB Magnets without Mechanical Pretreatment by Sulfuric (H<sub>2</sub>SO<sub>4</sub>) and Hydrochloric (HCl) Acids. *Minerals* **2021**, *11*, 1374. [[CrossRef](#)]
21. Orefice, M.; van den Bulck, A.; Blanpain, B.; Binnemans, K. Selective Roasting of Nd–Fe–B Permanent Magnets as a Pretreatment Step for Intensified Leaching with an Ionic Liquid. *J. Sustain. Metall.* **2020**, *6*, 91–102. [[CrossRef](#)]
22. Efstratiadis, V.; Michailidis, N. Sustainable Recovery, Recycle of Critical Metals and Rare Earth Elements from Waste Electric and Electronic Equipment (Circuits, Solar, Wind) and Their Reusability in Additive Manufacturing Applications: A Review. *Metals* **2022**, *12*, 794. [[CrossRef](#)]